# Cross-Strand Coupling and Site-Specific Unfolding Thermodynamics of a Trpzip $\beta$-Hairpin Peptide Using $^{13}C$ Isotopic Labeling and IR Spectroscopy

**Rong Huang,[†,§] Ling Wu,[†] Dan McElheny,[†] Petr Bouř,[‡] Anjan Roy,[†] and Timothy A. Keiderling*[,†]**

*Department of Chemistry, University of Illinois at Chicago, 845 W. Taylor Street (m/c111), Chicago, Illinois 60607-7061, and Institute of Organic Chemistry and Biochemistry, Academy of Sciences, Flemingovo nam. 2, 16610, Prague, Czech Republic*

*Received: February 16, 2009*

Conformational properties of a 12-residue tryptophan zipper (trpzip) $\beta$-hairpin peptide (AWAWENGKWAWK-$NH_2$, a modification of the original trpzip2 sequence) are analyzed under equilibrium conditions using ECD and IR spectra of a series of variants, singly and doubly $C_1$-labeled with $^{13}C$ on the amide C═O. The characteristic features of the $^{13}C$═O component of the amide I′ IR band and their sensitivity to the local structure of the peptide are used to differentiate stabilities for parts of the hairpin structure. Doubly labeled peptide spectra indicate that the ends of the $\beta$-strands are frayed and that the center part is more stable as would be expected from formation of a stable hydrophobic core consisting of four tryptophan residues, and supported by MD simulations. NMR analyses were used to determine a best fit solution structure that is in close agreement with that of trpzip2, except for a small variation in the turn geometry. The distinct vibrational coupling patterns of the labeled sites based on this structure are also well matched by ab initio DFT-level calculations of their IR spectral patterns. Thermal unfolding of the peptides as studied with CD spectra could be fit with an apparent two-state transition model. ECD senses only the tryptophan interactions (tertiary-like) and their overall environment, as shown by TD-DFT modeling of the Trp−Trp $\pi-\pi^*$ ECD. However, variation of the amide I IR spectra of $^{13}C$-isotopomers showed that the thermal unfolding process is not cooperative in terms of the peptide backbone (secondary structure), since the transition temperatures sensed for labeled modes differ from those for the whole peptide. The thermal data also evidence dependence on concentration and pH but these cause little spectral variation. This study illustrates the consequences of multistate conformational change at the residue- or sequence-specific level in a system whose structure is dominated by hydrophobic collapse.

The simplest $\beta$-sheet unit is a $\beta$-hairpin, in which two antiparallel $\beta$-strands are connected by a reverse turn (usually 2−6 residues). Studies of isolated, water-soluble $\beta$-hairpins can provide valuable insight into properties of $\beta$-sheet structure and folding since $\beta$-hairpins are considered to act as possible nucleation sites for protein folding.[1−14] Additionally, their detailed structural interactions can be relevant in developing an understanding of the mechanism for forming various $\beta$-sheet structures such as found in many (amyloid-like) neurodegenerative diseases in which protein aggregation is an important pathology.[15−18] During the past decade, there have been many reports discussing de novo designed, water-soluble $\beta$-hairpin peptide systems, as well documented in several reviews.[9,19−22] Among them, a $\beta$-hairpin peptide template, termed tryptophan zipper (or trpzip), which has four Trp residues forming a stable hydrophobic cluster in a hairpin formed from a sequence of 12−16 residues, has been the focus of a number of experimental and theoretical studies.[1,23−34] These trpzip peptides are monomeric, water-soluble, and have a high population of $\beta$-hairpin structure and high thermal stability in aqueous solution. Cross-strand interactions between the Trp residues, normally considered to be hydrophobic in nature, stabilize the whole hairpin structure. Trpzip has been reported to be the smallest peptide sequence that has a tertiary structure without disulfide bonds or metal binding.[1]

The folding of $\beta$-hairpins has been proposed to be initiated either by a sequence of residues with high propensities to form turn structures which then bring the $\beta$-strands together ("zipping" mechanism)[35] or by nonbonded interactions between opposing residues on the strands that lead to hydrophobic collapse and enable cross-strand hydrogen bond formation and subsequent turn formation.[10] Trpzip is an excellent model for study of such a hydrophobic collapse, which has been shown to contribute to its structural stability and the heterogeneity of its folding dynamics.[33]

Due to its sequence, trpzip is amenable for study with various spectroscopic techniques. It has a unique electronic circular dichroism (ECD) spectrum, arising from the exciton coupling of neighboring tryptophan residues, which can be used as a probe of Trp−Trp contact, and provide a measure of its tertiary structural stability.[1] Both static and dynamic fluorescence spectra can also monitor change of the tryptophan environment,[29,32] while IR absorption for the amide I band can be used to follow correlated secondary structural changes and dynamics during the unfolding process.[23,24,26,29,31,34,36,37]

Among the original trpzip sequences, trpzip2 has been more widely studied, partly due to simplicity and increased solubility.

* To whom correspondence should be addressed. E-mail: tak@uic.edu. Fax: (312) 996-0431.
[†] University of Illinois at Chicago.
[‡] Academy of Sciences, Prague.
[§] Current address: Department of Pathology and Laboratory Medicine, University of Cincinnati, Cincinnati, OH 45237.

10.1021/jp9014299 CCC: $40.75 
Published on Web 03/27/2009

From dynamic fluorescence studies, it was suggested that trpzip2 undergoes a rather complex unfolding process, indicating that this small peptide has a heterogeneous energy landscape.[32,33] T-jump IR spectroscopy has also been used to study its peptide backbone folding dynamics and confirmed the multistate nature of its thermal unfolding mechanism.[24,29,32,34]

IR is a powerful technique for sensing the peptide secondary structure, but due to its resolution limitations only average backbone conformational data can normally be determined. However, if combined with isotopic labeling, IR gains sensitivity to site-specific structural aspects of the peptide through vibrational coupling of selected residues which can be modeled using quantum mechanical (QM) force fields (FF) and atomic polar tensors (APT) for frequencies and intensities, respectively, as well as with empirical methods, as has been demonstrated by a number of applications.[38−43] Wang et al.[31] studied two single-labeled $^{13}C$ isotopomers of trpzip2 using linear and 2D-IR and concluded that the amide units are nondegenerate primarily due to solvent effects. Smith and Tokmakoff[27] have also used 2D-IR to study one doubly $^{13}C$-labeled trpzip2 peptide. Both studies demonstrated the potential of using 2D-IR for interpretation of vibrational coupling of labeled sites in peptides, but its full analysis is dependent on evaluation of the coupling constant characterizing these interactions, or equivalently on a theoretical model for the dispersion of the coupled modes. In addition, these authors also utilized this technique to monitor the local dynamics of this peptide.[28]

Thermal unfolding of small peptides is usually less cooperative than found for single-domain proteins. The resulting thermal denaturation curves are often characterized by very broad transitions.[43−47] Increase in the number of interstrand hydrophobic interactions has been shown to stabilize $\beta$-hairpin structures and result in somewhat more sigmoidal denaturation profiles in trpzips;[1,30,48] however, there can be a tendency for such peptide sequences to aggregate.[24]

Due to their small size, trpzips have also been a subject of many theoretical studies. One approach sought to simulate vibrational spectra for trpzips and provide structure−spectra correlations using QM FF methods.[40] Another is to study folding/unfolding [25,29,49] processes and solvation effects[50] by MD simulations. In this report, we combine both our QM spectral simulations to analyze changes during folding processes with equilibrium IR studies to extract local structural information from vibrational coupling evidenced in the $^{13}C{=}O$ amide I′ band and to explore the structural fluctuations that accompany thermal denaturation. Our MD analyses of various related hairpin structures will be reported separately (Kim and Keiderling, unpublished results). In an earlier report,[34] T-jump IR spectroscopic studies on the same labeled trpzip peptides were analyzed in terms of site-specific unfolding dynamics for these peptides. That work and the present studies taken together comprise an application of the now-developed methods of $^{13}C$ isotopic labeling in IR spectroscopy to provide site-specific resolution for a combination of equilibrium and dynamic IR techniques. Consequently, with the aid of theoretical modeling, this data can further our understanding of peptide structure and folding mechanisms at a residue-level, which may also be important for applied issues such as rational drug design or be extended to explore the relation between protein structure and genetic code variations. Here we provide the basic experimental, structural, and theoretical results underlying these thermal transitions in a modest variant of trpzip2.

**TABLE 1: Definition of the Trpzip Sequences and Labeling Positions in the Peptide Sequence with the Abbreviations Used in This Paper**

| abbrevn | peptide sequence[a] |
|---|---|
| trpzip1 | SWTWE*GN*KWTWK-$NH_2$ |
| trpzip2 (TZ2) | SWTWE*NG*KWTWK-$NH_2$ |
| TZ2A | SWAWE*NG*KWAWK-$NH_2$ |
| TZ2B | AWTWE*NG*KWAWK-$NH_2$ |
| TZ2C | AWAWE*NG*KWAWK-$NH_2$ |
| **A1** | **A**WAWE*NG*KWAWK-$NH_2$ |
| **A3** | AW**A**WE*NG*KWAWK-$NH_2$ |
| **A10** | AWAWE*NG*KW**A**WK-$NH_2$ |
| **A1A10** | **A**WAWE*NG*KW**A**WK-$NH_2$ |
| **A3K8** | AW**A**WE*NG***K**WAWK-$NH_2$ |
| **A3A10** | AW**A**WE*NG*KW**A**WK-$NH_2$ |

[a] Underlined (bold) residues are $^{13}C{=}O$ labeled on the amide C═O. Italics are the turn residues.

## Materials and Methods

**Peptides.** Ala (L-Alanine-N-Fmoc, 1-$^{13}C$, CLM-116) and Lys (L-Lysine-α-N-Fmoc, ε-N-T-Boc, 1-$^{13}C$, CLM-6194) were purchased from Cambridge Isotope Laboratories, Inc. All $\beta$-hairpin peptides, including the unlabeled, singly labeled, and doubly labeled peptides, were initially synthesized at the Protein Research Facility of the UIC Research Resources Center, using standard peptide synthesis protocols. Subsequent samples made in-house using standard Fmoc chemistry methods gave consistent data. Samples were HPLC purified and their identities were confirmed by MALDI-MS. Table 1 summarizes the various labeling positions in the peptide sequence and corresponding abbreviations that will be used in this paper, and their relative positions are shown in Scheme 1.

For ECD experiments at pH 7, no lyophilization was necessary and purified peptides were directly used in 20 mM phosphate buffer (pH ∼ 7). Alternatively, the purified peptide was directly dissolved in $H_2O$ and titrated with HCl to obtain pH ≈ 2.

For IR experiments, the purified peptides were lyophilized against 0.1 M DCl in $D_2O$ to remove the residual trifluoroacetic acid (TFA), which can interfere with IR measurements. The lyophilized peptides were dissolved in $D_2O$, which results in an acidic solution (pH 2). For experiments at pH 7, this solution was neutralized with small aliquots of NaOD prior to the last lyophilization. The TFA absorbance (∼1672 $cm^{-1}$) was significantly diminished with respect to the amide I′ IR band of the peptide after acidic lyophilization.

**Thermal Unfolding Measurements.** For ECD experiments at pH 7, a peptide stock solution at ∼1 mg/mL in 20 mM phosphate buffer was diluted to ∼0.1 mg/mL (determined from UV absorbance) and placed in a 1 mm path length quartz cell (Starna, Inc.) for temperature-dependent measurements. The same conditions were used for ECD experiments at pH 2, with a concentration of ∼0.2 mg/mL (determined from UV absorbance). Some experiments were done at higher concentrations up to 7 mg/mL (the latter using an IR cell with $CaF_2$ windows and a 100 $\mu$m path) for a test of consistency. Far-UV CD spectra were acquired between 185 and 250 nm on a JASCO J-810 spectrometer using a scan speed of 50 nm/min with a bandwidth of 1 nm and response time of 2 s. Variable-temperature experiments from 5 to 85 °C (in steps of 5 °C) were controlled by flow through a cell holder from a NESLAB (Thermo) RTE7DP water bath using a ramp speed of 1 °C/min between and an equilibration time of 5 min at each temperature setting. Final TZ2C ECD spectra presented are an average of 8 scans

**SCHEME 1: Isotopic Labeled Variants ($^{13}C$ Substituted C=O Indicated in Red) of Trpzip2C Used for This Study**[a]

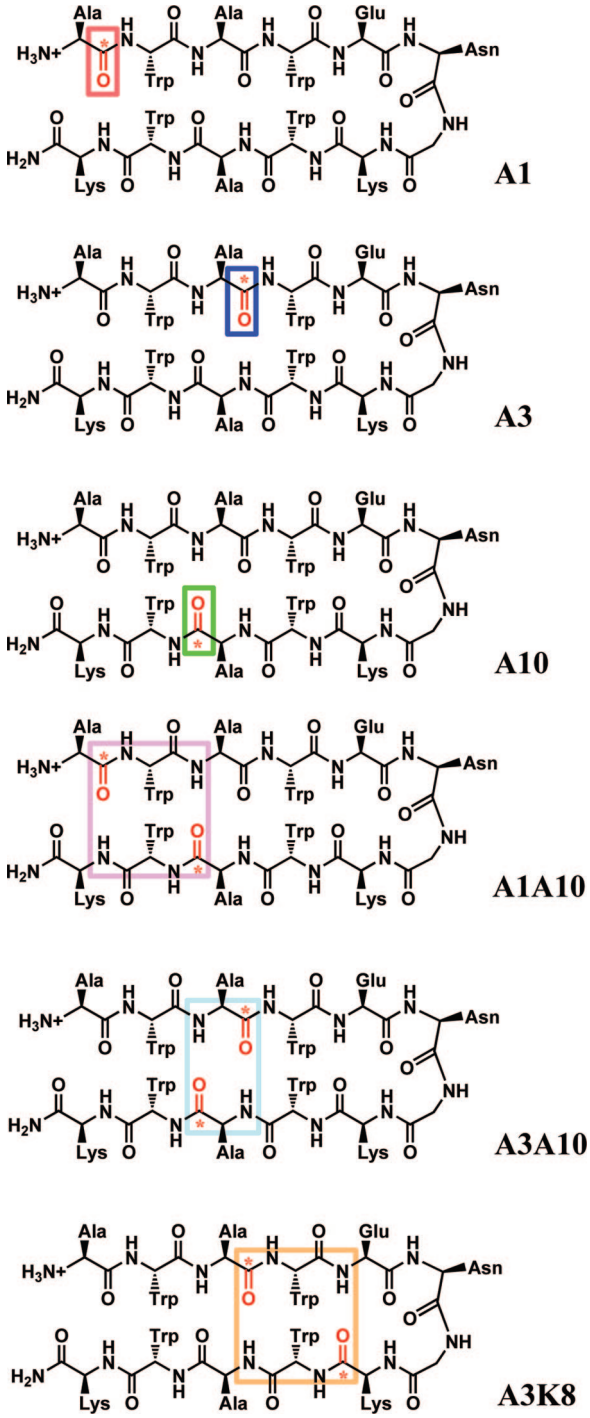


[a] The larger colored boxes indicate double-labeling patterns creating cross-strand H-bonded rings, termed "large" for A3K8 (also A1A10, but will be deformed due to fraying) and "small" for A3A10.

followed by subtraction of baseline spectra obtained under the same conditions. For near-UV CD spectra at pH 7, a more concentrated peptide solution and a 1 cm cell were used to enhance the weak signal, with the same spectral acquisition parameters as for far-UV CD spectra.

Samples for IR measurements at pH 7 were prepared at ~10−20 mg/mL in 20 mM deuterated phosphate buffer. Some samples were prepared under more dilute conditions (1 and 5 mg/mL) for concentration effect studies. The solutions were held in a homemade, brass demountable cell with $CaF_2$ windows separated by a 100 $\mu$m Teflon spacer, which was placed in a homemade cell holder connected to a NESLAB RTE 111 temperature bath. IR measurements were performed by heating the sample cell from 5 to 90 °C in discrete 5 °C steps and then cooling back to 5 °C. IR spectra were recorded on a DigiLab FTS-60A spectrometer (Randolf, MA) using DigiLab Resolution Pro for spectral scans. All the spectra were collected at a resolution of 4 $cm^{-1}$ with a zero-filling factor of 8. The sample was heated at a rate of 1 °C/min for 5 min, equilibrated for 11 min and then data was collected for 16 min (940 scans coadded) before the next temperature step. All sample spectra were subsequently baseline-corrected and corrected for any residual TFA absorbance (1672 $cm^{-1}$) remaining in the original spectra by subtraction of a reference spectrum.

**Thermal Spectral Analysis.** While multistate behavior for the folding of this hairpin has been established by dynamics studies, in order to compare with other equilibrium thermal unfolding and refolding data in the literature,[19,32−34] it is useful to approximate the observed transition by fitting the unfolding curves obtained from either IR or CD temperature-dependent spectra with a two-state model. Ideally, one can assume both the folded and the unfolded baselines change with temperature and that $\Delta C_p$ (change in heat capacity) may be nonzero. We tested this general model with various constraints to test for conditions under which we might obtain the best fits and most self-consistent results for these peptides, which are all actually the same molecule (TZ2C). We tested both flat and linear options in both the folded and unfolded thermal regions. In our studies, we found the best fits (those with lowest error) were usually obtained by use of a linear folded baseline and a flat unfolded baseline (slope = 0).[51] For TZ2, if both baselines were chosen to be flat, the errors in $\Delta H_m$ and $T_m$ became very large, and if both were linear, the $\Delta H_m$ and $T_m$ values were about the same, but the errors were much larger. Nonetheless, sometimes this larger error value can be more consistent for comparing behavior of related molecules. [Note: some previous studies used added denaturant to shift the transition to lower temperature and effect a more sigmoidal unfolding curve, which can yield more reliable fitting parameters, but this would impose a significant interference in the IR spectra.[32,33] Similarly, we did find that at reduced pH the $T_m$ values were generally lower, and the solubility at high temperatures was increased.] Also $\Delta C_p$ was set to zero in all the fits reported here since, in our hands, inclusion of this parameter in the model yielded small values with very large errors, but including it had little impact on $\Delta H_m$ and $T_m$ (<10% and <5 K).[51] Consequently $\Delta C_p$ should be viewed as undetermined or small, rather than equal to zero. The final equation for our modified two-state model to fit a temperature-dependent experimentally observable signal, $X$, is given as

$$X = \frac{(m_N T + b_N) + (m_D T + b_D)\exp\left[\frac{\Delta H_m}{R}\left(\frac{1}{T_m} - \frac{1}{T}\right)\right]}{1 + \exp\left[\frac{\Delta H_m}{R}\left(\frac{1}{T_m} - \frac{1}{T}\right)\right]} \quad (1)$$

where $\Delta H_m$ is the unfolding enthalpy evaluated at the transition midpoint temperature, $T_m$, $R$ is the gas constant, and $\Delta C_p = 0$. The remaining four parameters, $m_N$, $b_N$, $m_D$, $b_D$, represent the baseline parameters (slope and offset) for the assumed-linear, temperature-dependent changes of the native (N) and denatured (D) states, for which we have set $m_D = 0$.

The observable signal, $X$, was variously taken as CD intensity at a specific wavelength, IR amide I maximum frequency, IR intensity at a selected frequency, or coefficient of a component from singular value decomposition (SVD) analysis of the IR over the entire amide I band or some limited region, which gives the fits enhanced precision. These were all expressed vs temperature ($T$) and the fits analyzed in terms of the quality of fit as well as $T_m$ and $\Delta H$ values obtained. The variety of spectral analyses provided alternate views of the variation with $T$.

**Spectral Simulations.** Initial quantum mechanical (QM) IR spectral simulations were performed on a model $\beta$-hairpin peptide structure which was derived from intestinal fatty acid binding protein (PDB code: 1IFC) as previously reported and described in some detail in an earlier study of a different hairpin construct.[52] This computational model was able to predict the $^{13}C{=}O$ spectral features seen in experimental IR spectra for labeled $\beta$-hairpin peptides but, due to its idealized structure, failed to account for the $^{12}C{=}O$ amide I′ band shape. To explore the structural sensitivity of such spectral simulations, additional computations were done for fragments of a representative trpzip2 structure taken from the NMR structure of Cochran et al.[1,53] (see Supporting Information) and on the full peptide backbone from the TZ2C NMR structure. For all QM calculations, side chains, except for Gly, were reduced to Me (i.e., converted to Ala residues).

In the latter approach, the sequence, as taken from the TZ2C NMR structure determined in this study, was substituted to have methyl side chains (all-Ala representation) and optimized with constrained torsions. The result was used to directly compute spectral parameters (FF and APT) eliminating fragmentation. Computations were done at the 6-31G*/BPW91 level using a Linux-based machine with four 64-bit processors and shared memory (16 GB). The BPW91 functional is faster than the conventionally used hybrid functional (B3LYP) and for the amide I and II bands gives better results, as we have previously shown.[40,54] The resulting FF and APT tensors were transferred to our programs for spectral simulation and isotopic substitution.[55−57]

Comparison of these results provides a simulation of the spectra for models of the folded structure and some evaluation of the effects of distortion of the ideal hairpin geometry. These simulations for the ideal and the trpzip2 NMR structure were performed in vacuum and with additional computations for the NMR structure using a continuum solvent correction model (COSMO[58−60]) to evaluate general solvent effects on the spectra. However, while encompassing some solution effects, COSMO calculations do not include specific H-bonds or encompass side-chain shielding or peptide fluctuation effects.[40,41]

To model the electronic CD from the Trp residues, we additionally carried out a series of time-dependent-DFT (TD-DFT) CD calculations of the low-lying electronic states of monomers, dimers, and tetramers of indole rings constrained to some relative geometries as found for the Trp side chains in the NMR-determined TZ2C structure (which are functionally identical to those in trpzip2). For a variety of basis sets, solvent corrections, and for indoles with and without methyls, which might represent a connection to the peptide chain, we computed excited-state energies, transition intensities, and circular dichroism. This study and its ramifications for aromatic CD studies will be reported separately (A. Roy, P. Bour, unpublished results), but the general results support our interpretation, a summary of which is reported here.

**NMR Structure Analysis.** To confirm the similarity of the structure of our trpzip2 variant to the literature structure,[1,53] we measured the NMR spectra of both trpzip2 at 4 mM and trpzip2C at 6 mM concentrations in 90% $H_2O$ and 10% $D_2O$ at pH 5.8. Spectra used for the structure determination were acquired on a Bruker AVANCE 800 MHz spectrometer at 281 K with gradient selection and excitation sculpting for water suppression.[61] 2D NOESY were acquired (mixing times = 80 and 300 ms) with 12 ppm sweep widths, 2048 × 1024 complex points in $t_2 \times t_1$ and 16 scans per increment. 2D TOCSY were acquired under similar conditions with DIPSI2 mixing of 70 ms and an rf field of 8 kHz. In-phase COSY[62] was acquired under similar conditions as well to provide $^3J$(H,H) couplings and also aid in the assignment of the Trp rings. All spectra were processed within NMRPipe[63] and viewed/assigned in NMRView.[64]

The NOESY peaks were manually selected and assigned with CYANA 2.0.[65] The 100 lowest energy structures were selected from an ensemble of 500 and further refined by restrained MD using a previously described methodology within AMBER 8.[66] However, in this effort we used the ff99sb FF[67] and additionally employed the SHIFTS restraint[68] for the Trp rings with a force constant of 10 kcal/mol. Lastly, we report the resulting 20 unique structures with the lowest AMBER and restraint violation energies that were subjected to structure validation within PROCHECK_NMR.[69]

## Results

**Trpzip2 Variants.** Because of the low solubility of trpzip1, as found by us and others,[24,70] we focused our study on variants of trpzip2 (TZ2, which differs from TZ1 only in the turn sequence, see Table 1) as a template for these isotopic studies. In order to simplify isotopic labeling, we initially designed three variants of the original trpzip2 (termed TZ2A, TZ2B, and TZ2C in Table 1), which have various combinations of Ala substitutions at positions 1, 3, or 10 but keep the four interacting tryptophan residues intact.

The resultant ECD spectra for these variants are virtually identical to that previously reported for trpzip2 and have similar but somewhat reduced $T_m$ values on thermal unfolding,[1] and a reduced value at lower pH. In the far-UV region, these peptides have a negative (∼213 nm), then positive (∼227 nm), couplet band, which arises from exciton coupling of tryptophan residues on opposite strands.[70−72] These bands indicate that there are electronic coupling (exciton) interactions between residues Trp2-Trp11 and Trp4-Trp9, where they are arranged in an edge-to-face geometry. Our TD-DFT calculations support this interpretation (see Discussion and Supporting Information). The unique ECD signal from interactions of these aromatic residues can be used as a probe of tertiary structure (or cross-strand interaction) of the peptide upon unfolding (since the dipole coupling falls off with a distance dependence of $1/R^3$).

The amide I′ IR spectra of these peptides are also similar to that of trpzip2 and have roughly the same thermal unfolding profile when the change is followed in terms of peak frequency shift with $T_m \sim$ 344 K. However, if the absorbances at 1632 and 1652 $cm^{-1}$ which primarily sample $\beta$-strand and unordered parts of the structure, respectively, are followed separately to characterize the transition, the transition data encompass some variations. By contrast, if the full amide I band is used with an SVD-based analysis, the analyses of the fits result in more consistent thermodynamic parameters. To maximize labeling flexibility, and since it behaves well, we have chosen to use TZ2C for further isotopic substitution variations.

Our NMR results also support the high degree of structural similarity of the trpzip2 and trpzip2C folds. The chemical shift dispersion, determined as differences for the trpzip2 and

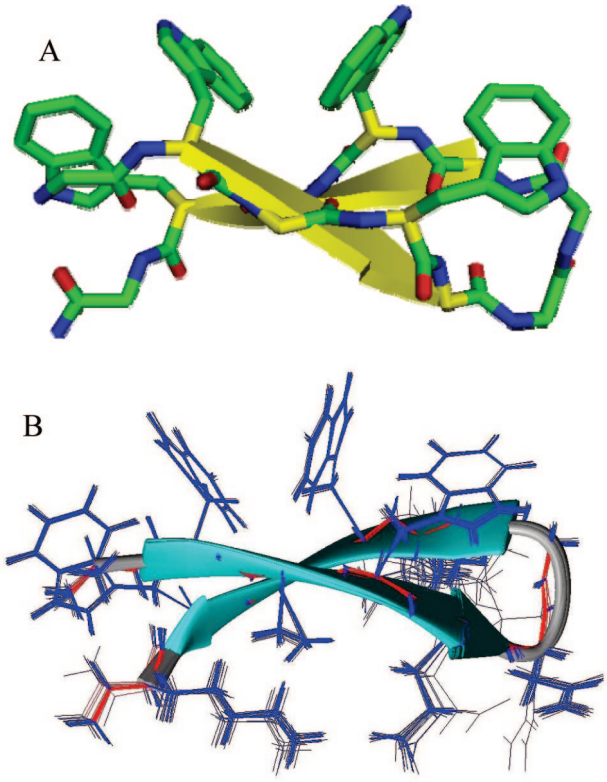


**Figure 1.** (A) Representative trpzip conformation taken from 20 best NMR structures determined for TZ2C, showing $\beta$-strand H-bonding (edge-on) and Trp side-chain interaction (pairwise, edge to face). (B) Overlap of 20 best structures on ribbon representation. Red indicates backbone. Glu5-Lys12 appear to form a salt bridge, and Lys8 is quite disordered (behind backbone in this representation).

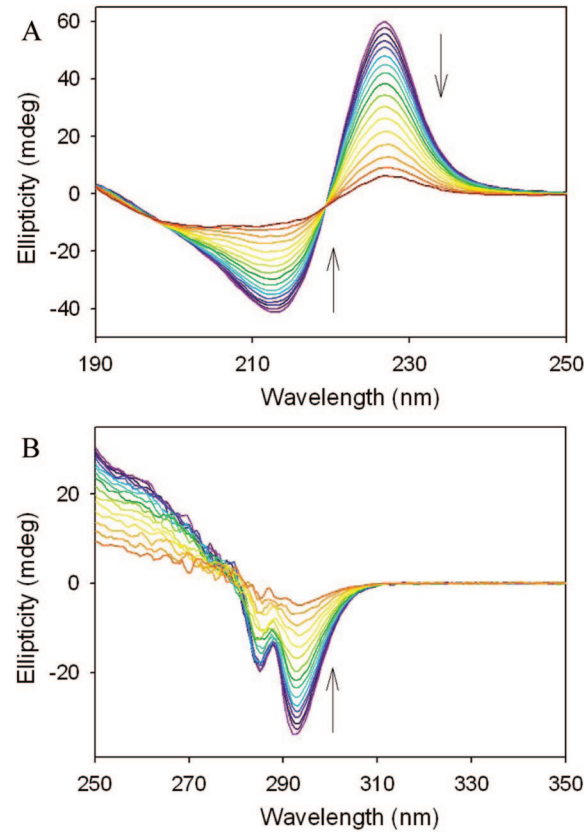


**Figure 2.** Temperature-dependent CD of TZ2C in (A) far-UV and (B) near-UV, both resulting from Trp−Trp interaction. Temperature increases from 5 (blue) to 85 (red) in steps of 5 °C. Near-UV data were obtained with increased concentration and path length to result in about 50 times more sensitivity. Molar ellipticity at 228 nm and 5 °C is about $10^6$ deg cm$^2$ dmol$^{-1}$.

trpzip2C $C_\alpha$-H resonances from the "random coil" values, show a clear pattern with the turn residues being negative (helix-like) and the central strand ones being positive ($\beta$-like) (see Supporting Information, Figures S1 and S2). To validate our structural determination methods, we first resolved the structure for trpzip2 with new NMR data obtained with our own samples and were able to confirm the result of Cochran et al., including the specific Trp−Trp interaction geometry.[53] Then we solved the TZ2C structure as described above, which yielded a hairpin structure, as shown in Figure 1, that is in close agreement with that of trpzip2. An overlap of the 20 best structures found in our NMR analysis for TZ2C indicates that the backbone and most side chains, especially the Trp residues, are well determined (see Figure 1B). The strand geometries of trpzip2 and trpzip2C are very close, both having a sharply twisted antiparallel $\beta$-sheet conformation. The aromatic side chains in TZ2C lie on one side of the hairpin with the same edge-to-face interaction as in TZ2 for W2−W11 and W4−W9. These residues are very regular, but the Lys8 side chain after the turn is relatively disordered (or poorly determined), while the terminal Lys12 and Glu5 are more ordered and appear to form a salt bridge in our structural solution. The turn conformation is in rough qualitative agreement with the original structure, but lacks a detailed overlap, since TZ2C has ($\phi$,$\psi$) torsional angles of (50°,43°), respectively, for Asn and (72°,25°) for Gly as compared to (71°,25°) and (82°,−2°) for trpzip2, and our initial structure solutions showed some variance in the best 20 structures. These TZ2C values can be viewed as being characteristic of a distorted type III′ turn, where ideally ($\phi$,$\psi$) = (60°,30°) for both residues, while trpzip2 is closer to a type I′ turn, ideally (60°,30°) and (90°,0°) (see Supporting Information for comparison data, Table S2). In summary, the NMR structural results confirm that the three Ala substitutions used to form TZ2C do not significantly change the cross-strand $\beta$-hairpin character determined in the structure of trpzip2.

**ECD Thermal Denaturation.** The CD spectra of TZ2C dramatically changes due to thermal unfolding as shown in Figure 2. These CD spectral shapes are pH independent, although a weak negative band does appear at ∼195 nm for pH∼2 peptides, see Supporting Information, Figure S5.A. Obviously, the intensities of the exciton-coupled bands in the far-UV region collapse upon heating, which is consistent with the Trp−Trp coupling rapidly weakening as temperature increases, as expected from the greater separation caused by unfolding. The near-UV CD spectra of TZ2C (Figure 2B) show a dominant negative band, indicating that at low temperature the tryptophan residues are located in a well-defined tertiary structure. These intensities decrease dramatically upon heating, which again is consistent with loss of tertiary structure (compact hydrophobic cluster) when unfolding. That both the near- and far-UV CD bands arise from coupled $\pi-\pi^*$ transitions of the Trp side chains is further confirmed by our TD-DFT results, in which the computed CD spectra for four indole rings constrained to the side-chain geometry found in our trpzip2C NMR structure qualitatively reflect the experimental CD (Figure 3). Both the couplet CD in the far-UV and the negative near near-UV band are predicted. Transition frequencies vary with basis set and functional used, but the spectral shape is quite stable.

The thermal unfolding process can be analyzed in terms of ellipticity changes vs temperature to determine a transition

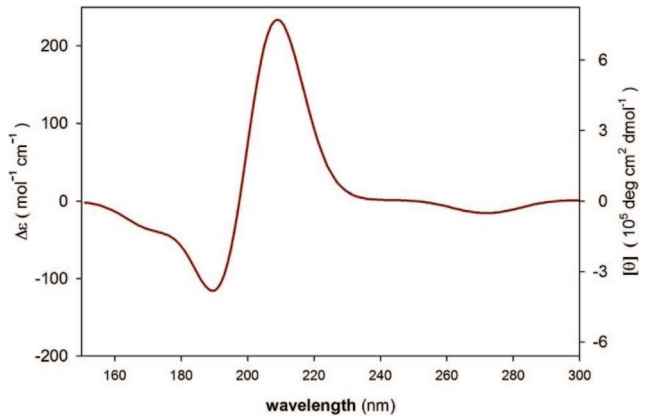


**Figure 3.** Simulated CD in the UV region for four indole rings constrained to the Trp side-chain geometries as obtained with TD-DFT calculations at the B3LYP/6-31G** level in vacuum. Both the $\pi-\pi^*$ coupling (predicted to form a dominant couplet at ~190−210 nm) and the n$-\pi^*$ transition (computed as a weak negative band at ~270 nm) are slightly high in frequency but in excellent agreement with experimental intensity patterns (blue, low-temperature traces in Figure 2, A and B, respectively), confirming pairwise interaction of the cross-strand coupled Trp side chains as the source of the far-UV CD.

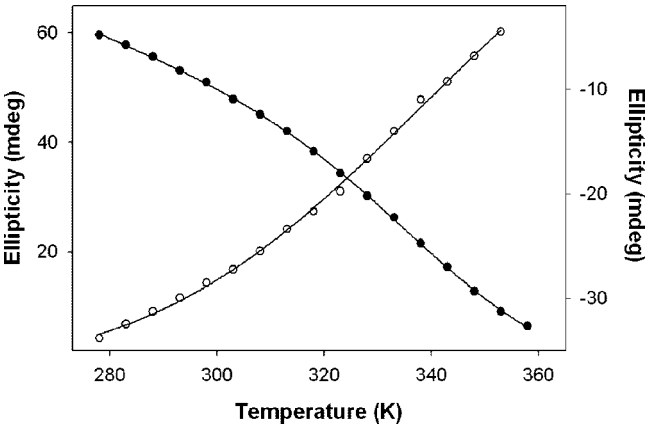


**Figure 4.** Comparison of temperature dependence for CD intensity of trpzip2C at 227 cm$^{-1}$ (far-UV, positive band of couplet, filled circles, left scale) and 293 cm$^{-1}$ (near-UV band, open circles, right scale). These yield approximately the same $T_m$ values: 347 ± 1 K (far-UV) and 350 ± 10 K (near-UV).

temperature. For example, the ellipticity decrease of the band at ~227 nm with increasing temperature is shown in Figure 4 (filled circles). From the fit to a two-state model, the transition temperature ($T_m$) of TZ2C is found to be similar to that of trpzip2 (see Table 2, however; our remeasurement of the trpzip2 CD yielded a somewhat higher $T_m$ than reported, which is probably indicative of a difference in the experimental method, we collected full spectra and took the intensity from them, or of fitting errors in the models used). Using the same measurement and fitting methods, $T_m$ for TZ2C was consistently somewhat lower than for TZ2, indicating a small reduction in stability, which provides an advantage to our mutation for thermal unfolding studies. At lower pH, the transitions also occur at consistently lower $T_m$ values for both TZ2 and TZ2C. In our experience the reproducibility error for repeated measurements of the transition is significant and not reflective of the much lower statistical error of the individual fits. The ellipiticity changes at both 213 and 227 nm have the same $T_m$, as expected for CD of exciton-coupled bands. The $T_m$ derived from ellipticity changes at ~293 nm is less reliable, but is consistent with the far-UV value (Figure 4, "open symbols"). From the results of these fits, summarized in Table 2, the three amino acid mutations to Ala at positions 1, 3, and 10 did not significantly change the structure or thermal behavior of TZ2C.

Additional tests were done to detect any impact of intermolecular interaction on spectral data by means of varying concentrations. The band shapes for the ECD spectra do not change with concentration, for concentrations over a range from 0.1 mg/mL up to 7 mg/mL, which is possible by comparison of data obtained with conventional quartz cells for low concentrations and IR cells ($CaF_2$ windows) with 100 $\mu$m spacers for high concentrations (see Supporting Information, Figure S6A). The intensities agree within the sort of error expected for IR cells, whose path lengths are somewhat variable. At the higher concentration values, absorbance of the peptide (plus solvent) prevents our obtaining CD for the high-frequency (low-wavelength) component band and above that reliable CD measurements are not possible. In terms of temperature variation, increasing concentration does not affect $T_m$ values very much, shifting up $T_m$ from ~340 to ~344 K at 7 mg/mL, which is coupled to a decrease of $\Delta H$ from ~17.1 to 13.6 kcal/mol (Table 2). These parameters may be impacted by concentration error, but the systematic changes indicate that error is small (see Supporting Information, Figure S6B). Changes in pH and other external conditions also impact $T_m$, so that variations in values obtained with different techniques are expected. The important aspect for comparison of these data analyses are thus the relative, systematic changes observed for related molecules.

**IR Thermal Denaturation.** At $T$ = 5 °C, the $^{12}$C amide I′ intensity maximum for unlabeled TZ2C is at ~1633 cm$^{-1}$ (as compared to ~1636 cm$^{-1}$ for trpzip2), which is consistent with a cross-strand, hydrogen-bonded $\beta$-strand conformation. Except for **A1**, whose $^{12}$C amide I′ frequency is ~1630 cm$^{-1}$, all the other labeled peptides have a higher $^{12}$C amide I′ frequency (about 4−6 cm$^{-1}$) than does TZ2C. This corresponds to a disruption of the $^{12}$C═O exciton coupling in the strands arising from the $^{13}$C═O oscillator(s) placed in the strand sequence. Since **A1** is a terminal residue, it does not impact the intrastrand coupling. This exciton coupling is the source of the characteristic $\beta$-sheet IR bands.

The low-temperature IR spectra of the $^{13}$C-substituted TZ2C peptides show an additional peak on the low-frequency side of the amide I band, with two variations worth pointing out. First, although the $^{13}$C peak in the spectrum of **A1** may not be obvious, the effect of isotopic substitution is clear in the difference spectra and in the second derivative of the original spectra (data not shown). Second, **A1A10** has two $^{13}$C peaks (shoulders) rather than a single peak as seen in either **A3A10** or **A3K8**, and in the other singly labeled species.

The amide I′ IR spectra of the unlabeled and singly labeled peptides measured as a function of temperature in 20 mM phosphate buffer are shown in Figure 5. For all peptides when heated to 85 °C (358 K), there is a gradual loss of peak intensities in both $^{12}$C and $^{13}$C bands and a shift of the $^{12}$C band to higher frequency, indicating a thermal transition from a $\beta$-hairpin to a more disordered secondary structure conformation. The variances seen at low temperature are lost at high temperatures so those band shapes for the labeled peptides are quite similar, although the $^{13}$C═O band is still detectable, even for one residue, which indicates that the labeled amides have become more equivalent in the disordered structure. These changes are accompanied by loss of tertiary structure as confirmed by both far-UV and near-UV CD spectra.

The thermal unfolding IR spectra for the doubly labeled peptides are shown in Figure 6. Again, similar changes in

**TABLE 2: Transition Temperature Variation with pH and Concentration, from Far-UV CD and IR**

| | pH study | | concentration study[b] | | |
|---|---|---|---|---|---|
| abbrevn | $T_m$ (K) at neutral pH | $T_m$ (K) at acidic pH | concn (mmol) | $T_m$ (K) | $\Delta H_m$ (kcal/mol) |
| trpzip2[a] | 352 ± 2 | 343 ± 1 | 0.15 | 340 ± 0.6 | 17.1 ± 0.9 |
| TZ2C | 347 ± 1 | 336 ± 1[b] | 0.35 | 342 ± 0.6 | 15.9 ± 0.7 |
| TZ2C (near-UV)[c] | 350 ± 10 | – | 4.46 | 345 ± 1.6 | 13.6 ± 1.6 |
| TZ2C (IR/SVD)[d] | 342 ± 0.6 | 332 ± 1 | | | |
| TZ2C (IR/intens)[d] | 340 ± 1 | 333 ± 3 | | | |

[a] Remeasured data for 227 nm, which is also consistent with Cochran's original data ($T_m \sim 345$ K, pH 7).[1] Indicated errors represent quality of statistical fits, not repeat measurements. [b] TZ2C-**A3K8** thermal ECD data at pH ~ 2, and concentration data are for TZ2C-**A3A10** monitored at 227 nm. Isotopes do not affect CD. [c] Near-UV monitored at 293 nm is obtained in longer path cell and was not measured for low pH. [d] Amide I IR for TZ2C analyzed using variation of second component from SVD of whole band or peak intensity at 1636 $cm^{-1}$.

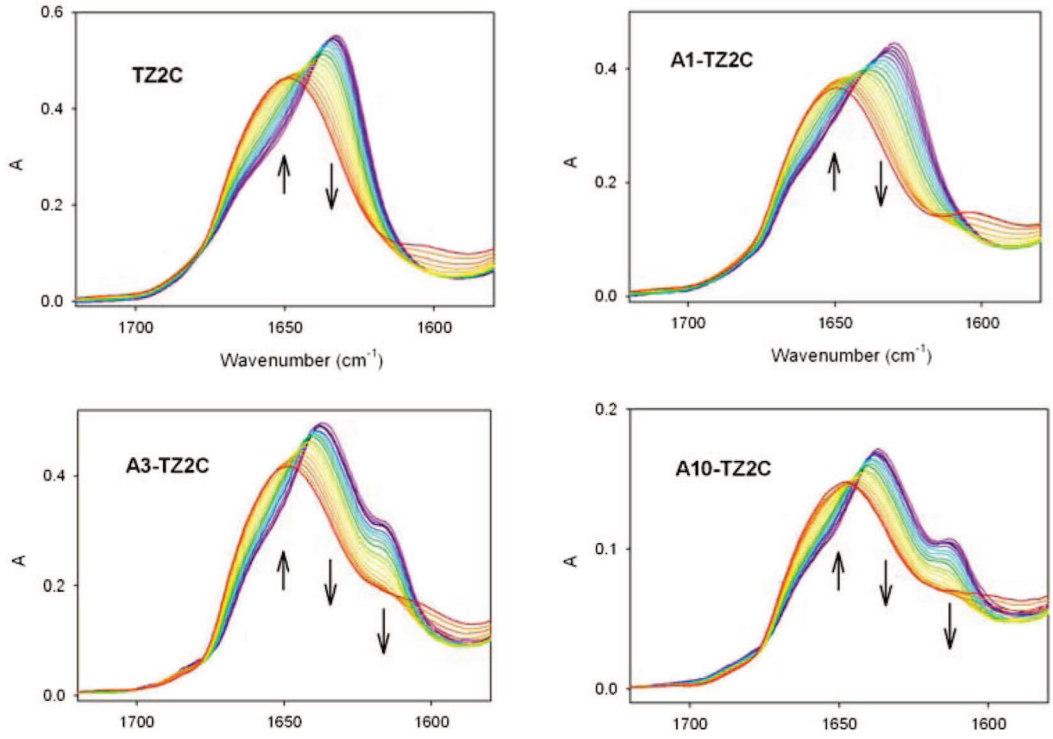


**Figure 5.** Temperature variation of amide I′ IR spectra of the unlabeled and singly labeled TZ2C. Three variants, **A1, A10, A3** plus unlabeled trpzip2C, are indicated. Temperature increases from 5 (blue) to 90 (red) in steps of 5 °C (278 to 363 K).

spectral features are seen for these peptides, except that the variations between labeling patterns are much more distinct than for single labels and the **A3K8** has a much larger loss of $^{13}C$ peak intensity with increase in temperature as compared with **A1A10** and **A3A10**. The $^{13}C{=}O$ intensity enhancement in the double-label examples is much more than one would expect for an additive effect in comparing two vs one labeled residue, suggesting that the pattern variations arise from cross-strand coupled amides whose transition dipoles have different interactions with the entire peptide.

While these spectral variations are clear and systematic, their interpretation is generally dependent on fitting the variation of measurable spectral parameters to a thermodynamic model. Variations of the $^{12}C$ amide I′ frequency shift (Figure 7) for both heating and cooling (Supporting Information, Figure S7) were analyzed using a two-state model. Particularly at neutral pH, the cooling values are less reliable, although the $T_m$ values are generally comparable for heating and cooling, yielding a reproducibility within ~5 K for TZ2C frequency shift $T_m$ values. The separate $^{12}C$ peak intensities (see Supporting Information, Figure S8, for which the unlabeled TZ2C result is about the same shape as for **A1**) were also fit to this model and show a fairly good agreement between frequency and intensity fits, as summarized in Table 3. The fits for some of the $^{12}C$ intensity variations were problematic since those plots were not sufficiently sigmoidal, but the frequency fits provide an alternate means of monitoring the $^{12}C$ transitions. For the $^{13}C{=}O$ modes, intensity is the only useful variable, and the results of their fits are shown in Figure 8 and compared to the $^{12}C$ values in Table 3. $T_m$ values varied more for fits to intensity than to frequency variation and also depended somewhat on the fitting model used. The $^{12}C{=}O$ fits gave about the same $T_m$ with both models tested, but some fits were unreliable using both linear baselines. For the $^{13}C{=}O$ intensity results at neutral pH, the $T_m$ and $\Delta H_m$ values for fits with linear-folded and flat-unfolded baselines baselines were within one standard deviation of the fit values obtained using both linear baselines (see Table 3, last columns), although the latter had larger errors, particularly for $\Delta H_m$. The $^{13}C{=}O$ variances probably result from temperature dependence of the residual water absorbance bands, which impact these lower frequency band differently.

To address these inconsistencies and the weakly sigmoidal shapes, we carried out singular value decomposition (SVD, or equivalently a principal component) analysis of the entire amide I region to separate average and variable spectral parts. This effects an averaging and noise reduction that results in improved

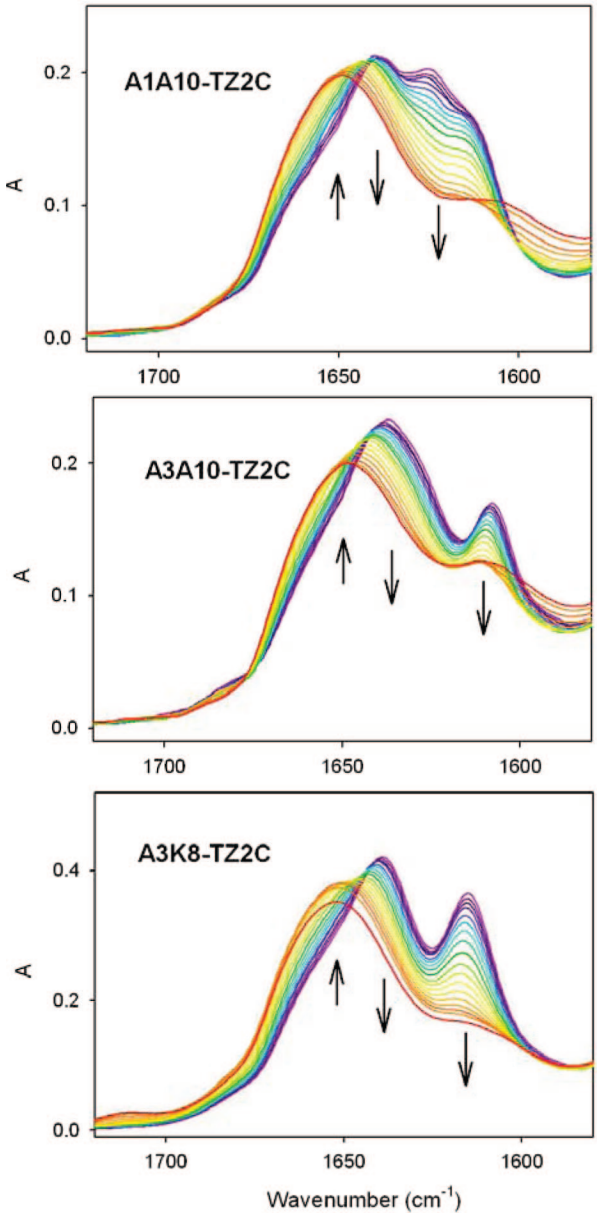


**Figure 6.** Amide I′ IR spectra of the doubly labeled TZ2C variants as function of temperature. Data for **A1A10**, **A3A10**, and **A3K8** are presented top to bottom, where temperature increases as in Figure 5.

fits. The thermal variation of the coefficient of the second spectral component was fit to a two-state model. [The first component had only a small variance with temperature, as normal for IR spectra.] These thermal variations (see Figure 9) were more sigmoidal, appeared more uniform, had fits with less error, and gave more consistent $T_m$ values than did the single-frequency intensity variation results. In particular, the **A1A10** and **A3A10** results closely overlap the **A10** curve while the **A3K8** differs and all differ from **TZ2C**. The resultant parameters are summarized in Table 4. To separate contributions, the SVD were also computed for the $^{12}C$ and $^{13}C$ regions of the amide I, a method which is only approximate at best. The $^{12}C$ results tracked the whole band results but on average were higher, but the $^{13}C$ SVD results were of lower reliability, due to overlap with baseline fluctuations presumably caused by residual solvent absorbance, and were not used further.

**Spectral Simulation Results.** To understand the spectra−structure correlation better for the studies of these peptide models and to explore the effect of $^{13}C$-labeling patterns on vibrational

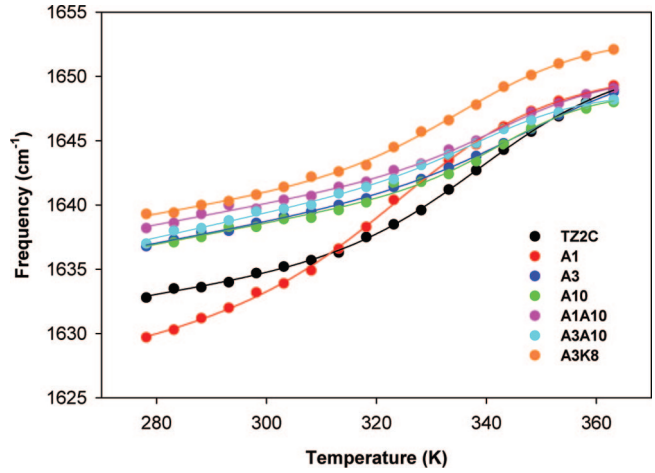


**Figure 7.** $^{12}C$ amide I′ IR frequency shift with increasing temperatures for all TZ2C-derived peptides. Transition temperatures obtained are listed in Table 3.

coupling, we have simulated the IR spectra at the QM-DFT level. Calculations used both an idealized model $\beta$-hairpin (derived from an antiparallel $\beta$-sheet structure in intestinal fatty acid binding protein, PDB code 1IFC, but all residues converted to Ala) and one based on the TZ2 NMR structure.[1] Both used force field (FF) and intensity (APT, atomic polar tensor) parameters computed at a DFT level for smaller constructs which were then transferred onto the larger target molecule. Additionally, a full DFT calculation using the TZ2C NMR structure, as determined here, was carried out, again for an all-Ala variant. Figure 10 provides a comparison of some of these theoretical predictions for the amide I IR for the doubly labeled and unlabeled peptides with the ideal structure (Figure 10a) and with a full DFT calculation for the **TZ2C**-NMR structure (Figure 10b), which can be contrasted with the corresponding experimental results (Figure 10c). (Additional computed spectral results for these variants are available in the Supporting Information, Figure S10.)

As typical for peptide DFT calculations, the computed amide I frequencies for both the ideal and NMR structure in vacuum are much higher (~50 $cm^{-1}$) than seen experimentally. This is largely due to the lack of solvent effects in the computation, and in part is a consequence of the DFT-derived FF.[38,54,73] The relative intensity and frequency patterns for the $^{13}C{=}O$ bands are primarily due to the coupling between residues (off-diagonal FF) and are mostly unaffected by this diagonal FF (frequency) error, resulting in good qualitative agreement with experiment for **A3A10** and **A3K8**, although the two low-frequency features in **A1A10** are not reproduced in the computed spectra for either the ideal or the NMR structures. The model structures have no fraying, since they are fully ordered in the ideal case and have a unique, although not fully regular, structure in the NMR case (Figure 1), which impacts the A1 position the most. The computed components of the $^{12}C{=}O$ bands for the ideal structure are also more resolved than seen experimentally for the same reason, and, in part, due to differentiation between H-bonded C=O groups and those that are directed out into the vacuum in the calculation, but are H-bonded to $D_2O$ in the experimental, solvated conditions. By necessity, these frozen structure calculations can not reflect the variations that characterize the ensemble of structures that exist for the real hairpins where the termini are partially unfolded, thereby sampling many local conformers, and where the turn is somewhat distorted and all residues are solvated. All that said, they do reproduce very well the

**TABLE 3: Thermodynamic Transition Temperatures ($T_m$) and Enthalpies ($\Delta H$) from Two-State Model Fits to Amide I IR Frequencies and Intensities[a]**

| | $^{12}$C frequency | $^{12}$C intensity | | $^{13}$C intensity | | | |
|---|---|---|---|---|---|---|---|
| | | | | linear−flat[d] | | linear−linear | |
| abbrevn | $T_m$ (K) | $T_m$ (K) | $\Delta H$ | $T_m$ (K) | $\Delta H$ | $T_m$ (K) | $\Delta H$ |
| trpzip2 | 351 ± 4 | 352 ± 3 | 15 ± 3 | – | – | | |
| TZ2C | 345 ± 1 | 340 ± 1 | 12 ± 1 | – | – | | |
| **A1** | 331 ± 2 | 330 ± 2 | 12 ± 1 | n.d.[b] | n.d.[b] | | |
| **A3** | 351 ± 2 | 347 ± 2 | 15 ± 2 | 332 ± 1 | 22 ± 2 | | |
| **A10** | 348 ± 5 | 338 ± 2 | 18 ± 3 | 327 ± 2 | 26 ± 4 | | |
| **A1A10** | 348 ± 4 | 351 ± 2 | 17 ± 2 | 334 ± 2 | 15 ± 1 | 334 ± 5 | 15 ± 3 |
| | | | | 331 ± 1 | 23 ± 2 | 331 ± 3 | 22 ± 3 |
| **A3A10** | 345 ± 2 | 349 ± 2 | 17 ± 2 | 328 ± 2 | 36 ± 7 | 328 ± 3 | 34 ± 11 |
| **A3K8** | 341 ± 2 | n.d.[c] | n.d.[c] | 325 ± 3 | 13 ± 1 | 321 ± 2 | 19 ± 3 |

[a] The $^{12}$C frequency and intensity fit results reported here use eq 1 with linear folded and flat unfolded baseline, $\Delta C_p = 0$. $\Delta H$ in units of (kcal/mol). [b] No obvious $^{13}$C peak is seen. [c] Fit was unreliable due to lack of sigmoidal curvature. [d] The $^{13}$C intensity variation was fit using eq 1 with a linear folded and flat unfolded (left) and both linear (right) baselines for comparison.

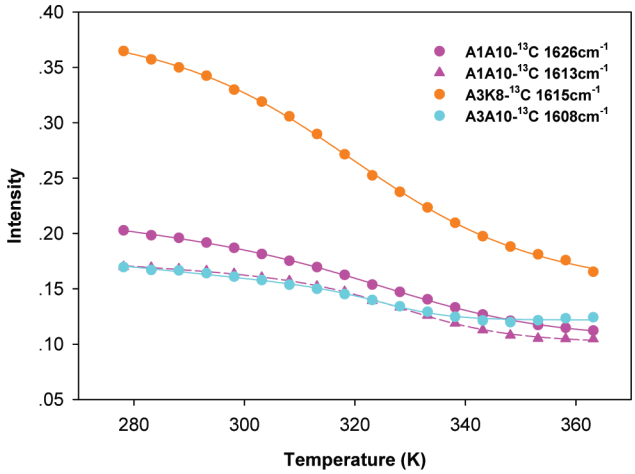


**Figure 8.** $^{13}$C amide I′ IR intensity change at the indicated wavenumber with increasing temperature for labeled peptides. Solid dots are $^{13}$C peak intensities, and associated lines of the same color indicate fits to a two-state model. Transition temperatures obtained from the heating cycle as determined using both linear-flat and linear-linear baselines are listed in Table 3.

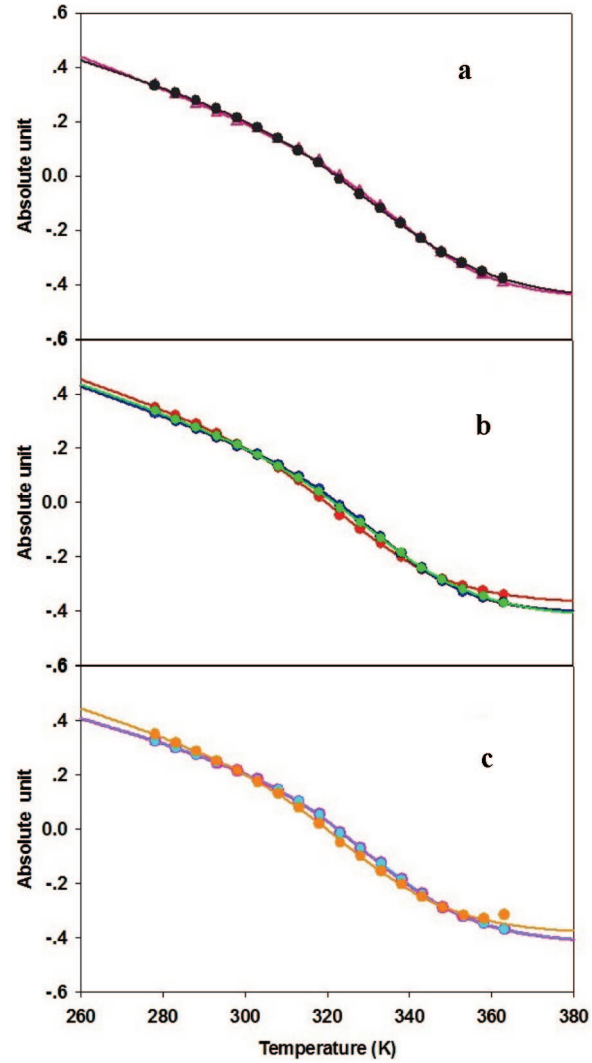


**Figure 9.** Thermal variation of the coefficient of the second component spectrum from SVD analysis of the amide I IR intensity for the entire band: (a) comparison of **TZ2** (triangles) and **TZ2C** (black dots); (b) **TZ2C-A1** (red), **TZ2C-A3** (blue), and **TZ2C-A10** (green); and (c) **TZ2C-A1A10** (pink), **TZ2C-A3A10** (cyan), and **TZ2C-A3K8** (orange). Fits to two-state model are shown as lines in the same colors.

qualitative patterns seen experimentally, especially for the labeled modes. These data are summarized in Table 5.

As we previously demonstrated,[40,41,52,54,74] the labeling patterns used for **A3K8** and **A3A10**, forming larger (14-atom) and smaller (10-atom) cross-strand $^{13}$C-labeled H-bonded rings (see Scheme 1) develop two distinct $^{13}$C═O vibrational coupling patterns. In **A3K8** (large 14-atom ring), the $^{13}$C peak appears at a higher frequency and with greater intensity than in **A3A10** (small 10-atom ring). This was seen for the TZ2C variants both in experiment and simulation, which clearly demonstrates that the vibrational coupling is different in these two cases and coincidentally proves that the TZ2 hairpin folds in-register as designed and as seen in the NMR structure. However, in contrast to the results for the idealized theoretical model of **A1A10**, two $^{13}$C═O bands are observed when the labels are placed near the ends of the $\beta$-strands, as opposed to only one $^{13}$C peak (which primarily reflects the out-of-phase oscillation of the cross-strand coupled pair) as seen for the other double-label variants, where the $^{13}$C are located in the center part of the peptide strands. (The in-phase exciton component in a strongly coupled cross-strand pair would normally have very little intensity, since the dipoles would cancel.) This means that in **A1A10**, the labeled residues are decoupled and significantly nondegenerate, which is a direct consequence of the ends being frayed and the **A1** position being a terminal residue. This prediction is supported by our MD simulations of various hairpins, from which structures with varying degrees of frayed termini could be identified along a trajectory (Kim and Keiderling, unpublished results).

**TABLE 4: Thermodynamic Transition Temperatures ($T_m$) and Enthalpies ($\Delta H$) from Two-State Model Fits to Amide I IR Spectra Using SVD Analyses**

| | linear−flat[a] | | | | linear−linear[b] | |
|---|---|---|---|---|---|---|
| | SVD total | | $^{12}$C SVD | | SVD total | |
| abbrevn | $T_m$ (K) | $\Delta H$ | $T_m$ (K) | $\Delta H$ | $T_m$ (K) | $\Delta H$ |
| trpzip2 | 346 ± 0.7 | 19 ± 1.0 | – | – | – | – |
| TZ2C | 342 ± 0.6 | 15 ± 0.6 | – | – | 350 ± 7 | 13.5 ± 1.4 |
| **A1** | 333 ± 1.0 | 16 ± 0.7 | n.d.[b] | n.d.[b] | – | – |
| **A3** | 340 ± 0.5 | 19 ± 0.7 | 340 ± 0.5 | 20 ± 0.7 | – | – |
| **A10** | 340 ± 0.6 | 16 ± 0.7 | 341 ± 1.3 | 15 ± 0.9 | – | – |
| **A1A10** | 338 ± 0.7 | 17 ± 0.8 | 339 ± 0.6 | 17 ± 0.7 | 339 ± 4 | 16.6 ± 1.9 |
| **A3A10** | 337 ± 0.6 | 19 ± 0.7 | 338 ± 1.0 | 18 ± 1.0 | 337 ± 2 | 19.5 ± 1.7 |
| **A3K8** | 333 ± 1.3 | 16 ± 1.0 | 336 ± 1.3 | 14 ± 1.0 | 335 ± 6 | 14.8 ± 2.7 |

[a] Fit results reported here are for variation of the coefficient of the second SVD component using Eqn 1 with linear folded and flat unfolded baselines, $\Delta C_p = 0$. $\Delta H$ values in kcal/mol$^{-1}$. [b] These are compared to fits using linear baselines for both folded and unfolded states for selected cases (last two columns). [c] No obvious $^{13}$C peak is seen.

Computing the FF and APTs for the entire hairpin, all Ala, with the TZ2C conformation at the BPW91/6-31G** level in vacuum, without the need to approximate with fragments, results in predicted spectra with better agreement with experiment, as can be seen in Figure 10b. (Use of a hybrid functional leads to much worse absolute, but roughly the same relative frequency predictions as shown in the Supporting Information, Figure S10, A and B.) A similar calculation with a continuum solvent correction (COSMO) for the entire peptide did not converge. In particular, the variation in coupling constant and consequently the position of the peak of the $^{13}$C═O absorbance for the **A3K8** and **A3A10** large and small rings is still well predicted. The distortion in the NMR structure causes the in-phase component to have about half the intensity of the out-of-phase component, so the $^{13}$C═O bands tend to be broader and predicted with a shoulder. In most cases, the $^{12}$C═O modes reflect the pattern of the unlabeled species for the higher frequency amide I components, and the major variation in their pattern occurs for labels on **A3** and/or **A10** which are in the middle of the exciton coupled oscillators and thus disrupt the $^{12}$C═O coupling. The dispersion of the $^{12}$C═O modes in the full DFT NMR structure simulation is somewhat increased over that in the other calculations. Unlike the ideal case (Figure 10a) and in improved agreement with the experiment (Figure 10c), the **A1A10** $^{13}$C═O band predicted with the NMR structure is different, lying between the two cross-strand coupled models, **A3K8** and A**3A10** (Figure 10b). The predicted **A1A10** IR still does not exhibit the second band seen experimentally, but, since we computed a unique structure, rather than an ensemble, this is perhaps not surprising.

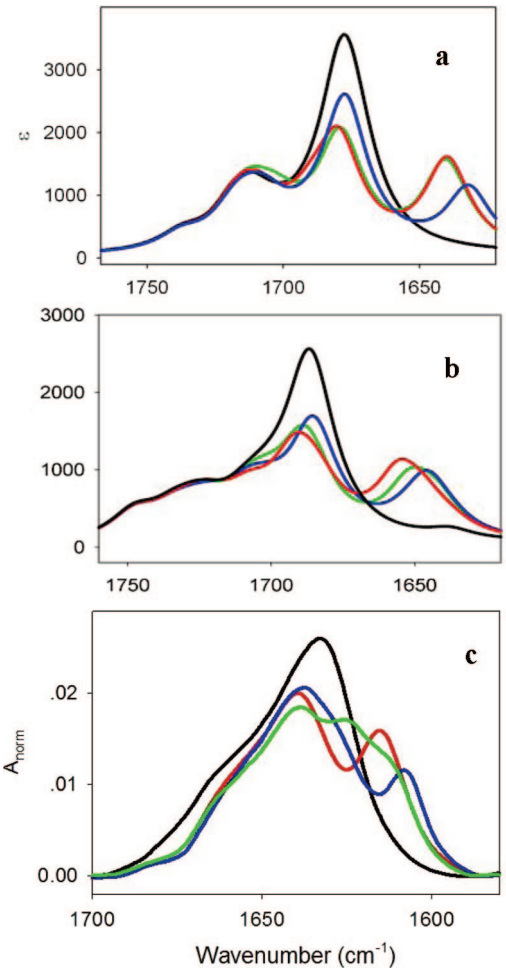


**Figure 10.** Comparison of (a,b) simulated IR spectra and (c) experimental IR spectra at $T = 5$ °C for **TZ2C** (black), **A1A10** (green), **A3A8** (red), and **A3A10** (blue). Simulations are presented for an all-Ala representation of the hairpin obtained from (a) a calculation for ideal hairpin, using transfer from segments of a protein $\beta$-sheet (**A3K8** and **A3A10** predicted to overlap) and (b) a full DFT calculation of the Ala-substituted sequence constrained to the trpzip2C backbone structure. All DFT calculations were done for the peptide in vacuum at the BPW91/6-31G** level with geometry optimization of local modes, but constraint of backbone torsions.

## Discussion

**Trpzip Variants.** The goal of this study was to use peptides related to trpzip2 as models for $\beta$-sheet formation via hydrophobic collapse and to explore the mechanism of structure formation by use of isotopic labels that allow IR spectra to provide site-selective information about the unfolding mechanism. While it is not critical that the peptide studied be precisely like trpzip2, as long as it has the hairpin fold with a dominant Trp−Trp interaction, it is useful that they are similar, since comparison can be made to several previous studies that have focused on trpzip2. The TZ2C modification enabled facile isotopic labeling studies while maintaining the desired $\beta$-hairpin structure, as we have shown through extensive spectral studies, including an NMR structure, comparing **TZ2C** with **TZ2**. The Ala substitutions have only small effects on the structure and on the resultant $\beta$-hairpin stability. All other properties map closely onto trpzip2 including CD and IR spectral band shapes and transition temperatures.

Qualitative NMR parameters for **TZ2C**, such as the chemical shift dispersion and differences from random coil values, are both consistent with $\beta$-hairpin structure and provide a very good match to the trpzip2 values. More directly, the $\beta$-strand segments of the two structures closely overlap and the entire structures are qualitatively identical (Supporting Information, Figure S4).[1,53] The main conformational difference is in the turn residues. The NMR structure shows a strongly twisted hairpin conformation (Figure 1) with the terminal residues having poor cross-strand H-bonds and the turn being closest to a type III′ $\beta$-turn with ($\phi$,$\psi$) at the $i + 1$ and $i + 3$ residues (Asn and Gly) of (51°,43°) and (72°,25°), respectively, approaching the ideal values of (60°,30°).

The four Trp residues in TZ2C interact pairwise with an edge-to-face side-chain ring orientation, with the same relative geometry but a somewhat tighter packing than in TZ2. This

**TABLE 5: Comparison of Experimental and Simulated Amide I IR Frequencies for an Ideal β-Hairpin Computation: Results for Labeled Peptides**

| | experiment[a] | | | ideal structure | | | TZ2C NMR structure | | |
|---|---|---|---|---|---|---|---|---|---|
| | | | | $^{13}$C modes[b] | | | $^{13}$C modes[b] | | |
| | $^{12}$C | $^{13}$C | $^{12}$C−$^{13}$C | asym | sym[d] | splitting | asym | sym[d] | splitting |
| Trpzip2 | 1636 | | | | | | | | |
| TZ2C | 1633 | | | | | | | | |
| **A1** | 1630 | n/a[c] | | 1636 | | | 1643 | | |
| **A3** | 1637 | 1615 | 22 | 1635 | | | 1647 | | |
| **A10** | 1637 | 1613 | 24 | 1637 | | | 1651 | | |
| **K8**[e] | | | | 1635 | | | 1655 | | |
| **A1A10** | 1638 | 1626 1613 | 12 25 | 1640 (25/mix) | 1632 (1/mix) | +8 | 1652 (11/A1) | 1643 (8/A10) | +9 |
| **A3A10** | 1637 | 1608 | 29 | 1632 (<1/mix) | 1640 (18/mix) | −8 | 1646 (13/mix) | 1654 (1/mix) | −8 |
| **A3K8** | 1639 | 1615 | 24 | 1640 (25/mix) | 1632 (<1/mix) | +8 | 1656 (13/K8) | 1647 (6/A3) | +9 |

[a] Frequencies (in cm$^{-1}$) are determined from the original spectra. [b] Frequencies of individual component normal modes (in cm$^{-1}$); the numbers in parentheses indicate relative intensity and assignment of local character in modes for double-labeled peptides; "mix" implies relatively equal distribution of the two labeled oscillators. [c] No obvious peak is seen. [d] The sym mode is weaker compared to the asym, since cross-strand coupled dipoles oppose each other. [e] K8 sample was not made experimentally, but calculated for comparison to other double-labeled peptides.

pairwise Trp−Trp interaction is the source of the characteristic derivative-shaped CD spectrum, which arises from exciton coupling of the $\pi-\pi^*$ transitions. TD-DFT calculations of a pair of indole rings constrained to the Trp side-chain positions found in the TZ2C NMR geometry yield such a couplet shape at about 200 nm and a weaker negative band at about 280 nm (Supporting Information, Figure S12), and four indoles constrained to the Trp side-chain positions yield a more intense pattern (Figure 3). The computed band positions shift with variations of basis set and substitution of the indole rings as well as correction for solvation, but the simulated spectral pattern is consistent and in excellent agreement with the experimental CD data. We have separately shown[70,72] that the Trp CD for the two Trp−Trp pairs in TZ2 is roughly additive and arises mainly from the cross-strand, pairwise interactions of residues 4 and 9 and 2 and 11, with less contribution from the stacked interaction between the pairs (2 and 9). The TD-DFT UV-CD computations bear this out.

**Site-Specific Vibrational Coupling.** As in our previous reports for β-hairpin isotopic labeling,[52,54,74] the **A3K8** and **A3A10** labeling patterns develop two distinct $^{13}$C═O amide I band characteristics. On the basis of our calculational models and the similarity with labeled amide I results for previously studied hairpins, we assign the differences to a sign change in the site-specific vibrational coupling interactions. For the large ring (where labeled H-bonded C═O groups form a 14-atom ring, exemplified by **A3K8,** see Scheme 1), the coupling constant is computed to be 4 cm$^{-1}$ (half the splitting in Table 4) resulting in the higher frequency component having a higher intensity, which for the less resolved experimental spectra would result in a smaller apparent shift of the $^{13}$C═O from the $^{12}$C═O band but yield more intensity. For the small ring (labels form a 10-atom H-bonded ring, e.g., **A3A10,** see Scheme 1) the opposite is true, the coupling being computed (ideal) as −4 cm$^{-1}$ with the intense mode lower in wavenumber than the weak one, thus yielding a larger apparent isotope shift.

In the spectral calculations based on the NMR structure, for both the spliced fragment and complete hairpin models, the local $^{13}$C═O modes are somewhat less coupled due to nondegeneracy of the underlying oscillators (more so for the fragment calculation), resulting in double-label coupling where both components have intensity. Even so, the same relative intensity pattern and phase relationship is computed for these modes in **A3A10** and **A3K8**. Again the higher frequency component is the more intense for **A3K8** (large ring), and the lower frequency $^{13}$C component of the amide I′ has greater intensity for **A3A10** (small ring), yielding agreement (more so for the full DFT calculation) with the experimental low temperature results (Figure 5 and 10c). The **A1A10** results are less coupled, more nondegenerate, but intermediate in predicted band position, which can also be seen to qualitatively agree with the experimental result.

The fragmentation may introduce end effects into the strand residues after transfer to the hairpin, which would distort the coupling in some pairs more than the others. The fact that the full peptide DFT calculation avoids this distortion supports such an interpretation. Of course, full DFT calculations are limited to smaller molecules, or to very large computational resources. From our fragmentation results, the COSMO calculations are seen to have band shapes for the $^{12}$C═O amide I modes in better qualitative agreement with experiment as well as improved frequencies. Our calculations do not give the anomalous behavior for **A1A10**, which experimentally shows two nondegenerate $^{13}$C═O peaks, although the full DFT calculation does predict the **A1A10** $^{13}$C═O band to lie between the **A3A10** and **A3K8** results, as seen experimentally. This extra $^{13}$C═O band in **A1A10** may be due to fraying of the hairpin termini, but our calculations are for a unique NMR structure, and even the ensemble of best such structures does not deviate enough from regularity to bring out such a spectral deviation. It is possible that this is a problem of the NMR method which uses a specific force field to miminize the structure, but it is also a problem of our use of a single structure to simulate spectra.

The shift of the local modes by ∼40 cm$^{-1}$ on $^{13}$C substitution of the amide tends to decouple the labeled modes from the rest of the hairpin strand amide I vibrations, but some residual mixing does remain, which must be the source of the difference in intensity for the large and small ring variations. It is the sign change in the coupling constant that is the major structurally related consequence seen in the spectrum, as we have shown with other species,[40,41,52,74] and that sign pattern lets us confirm the alignment of the strands as well as provides a structurally sensitive probe of the unfolding as temperature is increased. Although use of the NMR structure leads to more localized modes in our calculations, the coupling signs are the same as that evidenced by the intensity distribution, and they remain in overall agreement with experiment.

It is this real ensemble of structures, in a dynamic equilibrium, that probably lies at the basis for the ideal structure giving a qualitatively correct picture of the $^{13}C{=}O$ bands, when the peptide is labeled midstrand. The molecule is fluctuating and the contributions of the couplings to the termini and turn residues are averaged out so that the ideal picture retains its interpretive value. Such a model for the dynamic hairpin structure was supported by our MD simulations and is consistent with our reported T-jump relaxation kinetics for these same isotopically substituted trpzip2C hairpins.[34] Thus, the oscillators in the center of the strands have less nondegeneracy than the model predicts, as can be seen by the well-resolved $^{13}C{=}O$ bands in **A3K8** and in **A3A10**, which are clearly offset from each other, reflecting their oppositely signed coupling constants and a significant disparity in intensity for their in-phase (weak) and out-of-phase (intense) coupled modes than predicted with the NMR structure based spectral calculations. However, when labeled on the ends, the $^{13}C{=}O$ oscillators experience environments resulting in diagonal force field components not encompassed in the ideal model. Similarly, the $^{12}C{=}O$ modes always sample the termini and turn, so the replication of their spectra by single structure based calculations is hindered. Adding a correction for the dynamics of the water environment and for the peptide itself, by sampling an ensemble of related structures that allow for various distortions of the termini and the turn, would of course improve the spectral representation, but would also require a computational effort out of scale with the other approximations used in modeling the FF, such as ignoring the impact of side chains, which is a contribution that can lead to substantial shifts in the diagonal FF (A. Lakhani and G. Papadantonakis, unpublished results).

**Thermal Unfolding at Different pHs.** We have measured the thermal unfolding of the unlabeled **TZ2C** and selected labeled variants by ECD and IR at both neutral and acidic pH. Although the overall thermal unfolding profiles are very similar, there are two differences revealed by both methods: first, the unfolding/refolding reversibility is better in acidic pH than in neutral pH. Second, the transition temperatures derived from the unfolding profiles are lower in acidic pH than in neutral pH by about 10 K, as determined from our CD measurements (Table 2). The IR spectra at both pH values are similar in shape, as are the CD spectra, but the $^{13}C{=}O$ bands are slightly lower in frequency at low pH. The thermal changes are also similar, shifting and broadening the amide I band but yielding intensity variation vs temperature fits for the parent peptide at low pH with a lower $T_m$ than at higher pH (Table 2), which suggests that the peptide hairpin is less stable in acidic pH. While the absolute values for $T_m$ are different with CD and IR analyses, the trend is the same, lowering $T_m$ at low pH (Table 2). The thermal IR variation data for the acidic peptides were reported separately as part of our T-jump study.[34] Possibly consistent with this, at acidic pH, TZ2C shows a weak negative band at 195 nm which could be due to amide modes and might indicate increased contribution to the ensemble of structures from more disordered forms, presumably caused by more fraying at the termini, but the difference must be modest, given the similarity of the IR band shapes (see Supporting Information, Figure S5.A and S5.B), indicating that substantial $\beta$-strand interaction is maintained.

Another variable is concentration, which we have studied by making CD measurements for samples varying from 0.2 mg/mL (0.15 mM) to 7 mg/mL (4.5 mM) and IR measurements from 1 to 20 mg/mL. In all cases the spectral shapes were consistent, the CD virtually overlapped (Supporting Information, Figure S6A), with a small fall-off at high concentrations, which may be due to error in the short path length IR cell used for these tests. The lowest concentration IR spectra are not as reliable, since interference of solvent and effects of baseline fluctuations on amide I absorbances of the order of 0.01− 0.02 can severely affect band shapes with our instrument. The 5 mg/mL (3.2 mM) spectra ($A \sim 0.08$) were of the same shape and had a temperature dependence (for **A3A10**) that tracked the high concentration result but had a slightly lower Tm value (334 vs 338 K). The consistency of all the data make it clear that the molecules do not form different structures through aggregation at high concentrations, so comparison of CD and IR analyses are sensible. However, the environments are different (hence some variance in $T_m$ values), so that the analyses must be viewed as having quantitative limitations. Thus, trends for related systems, obtained under defined conditions, rather than precise thermodynamic values provide the most reliable interpretive results.

**Site-Specific $^{13}C$ IR Thermal Unfolding.** Our ECD results for the unlabeled TZ2C, just like trpzip2, suggest that the global thermal change of this peptide has apparent two-state transition characteristics. However, by sampling the IR spectrum at different wavenumbers, a variation in the $T_m$ values and differences in the nature of the transition curves is seen. Furthermore, from our isotopic study, the different transition temperatures and thermodynamic parameters obtained by monitoring the $^{13}C{=}O$ band transition with labeling at different sites make it clear that TZ2C cannot fold by a two-state mechanism. The differences in $T_m$ and $\Delta H_m$ with position of the isotopes suggest a lack of cooperativity that indicates different parts of the molecule have differentiable unfolding processes. Since these data are for molecules with the same structural energetics, such variations confirm a non-two-state behavior. Previous trpzip2 studies using CD or fluorescence could only detect the tertiary structure (Trp−Trp Interaction) change, which has one transition temperature for all these chemically identical species. However, the combination of $^{13}C$ labeling and infrared spectroscopy enable us to sense local sites and differentiate local unfolding. These results clearly suggest that the $^{13}C{=}O$ substitutions create oscillators with independent spectra that are sensitive to their local environment, but such probes are most useful if coupled to a second oscillator on the other strand so that their intensity reflects cross-strand coupling. This is in full agreement with our dynamic, T-jump IR, study which showed that the various labeled positions fold with different rates.[34]

In isotopic labeled IR measurements, we assumed that there is no change in the peptide thermal stability upon isotopic substitution and that the $^{12}C$ amide I′ band should report on the stability of the unlabeled peptide backbone, thus providing complementary information about the thermal stability of the local peptide backbone with labels. For example, the transition temperatures obtained from fits to either the $^{12}C$ amide I′ frequency shift or $^{12}C$ amide I′ intensity change are consistently higher than those from the $^{13}C$ amide I′ intensity change. This pattern suggests that the local thermal stability is somewhat "decoupled" from the global peptide stability. Furthermore, the $T_m$ values for the CD in general agree with the $^{12}C$ results, and are higher than the $^{13}C$ $T_m$ values, which further suggests that the local cross strand H-bond can open up before the tertiary interaction between the Trp side chains is lost, the latter of which destabilizes the entire hairpin.

The transition temperatures from $^{13}C$ intensity change fits can reveal some information about the relationship of label positions and relative stability. For example, since the **A1** $^{13}C{=}O$ is closer

to the end of the strands than that of **A10** or **A3**, its $T_m$ is lower. When comparing **A3A10** and **A3K8**, a different behavior is seen, in that **A3K8** always has lower $T_m$ values for $^{12}C$ or $^{13}C$ detected transitions. This behavior indicates a destabilizing influence of the turn, but also a coupling of the modes composing the $^{13}C$ and $^{12}C$ bands. This behavior is maintained in the more stable SVD analyses, yet results in a smaller difference, especially if focused on the $^{12}C$ component. But the apparent high $T_m$ from **A1A10** is obviously not consistent with our overall interpretation about the segmental stability along the peptide backbone.

## Conclusions

We have used a model $\beta$-hairpin peptide to determine the trpzip unfolding mechanism on a residue level and have correlated the thermally induced structural variations with NMR, IR, and CD spectral data. By consideration of structure variations and solvent effect, we have improved our ability to understand subtle spectral features. A key element of this improved understanding comes from the use of DFT based calculations of the vibrational spectra and TD-DFT calculations of the electronic spectra. Such detailed analyses of the spectra have not been previously available. Substitution of $^{13}C$ at various positions in $\beta$-hairpin peptide sequence allowed us to examine the vibrational coupling by sites; thus, this strategy provides an alternative yet attractive probe to study the peptide thermal unfolding dynamics at the residue level. Combining both equilibrium and dynamic IR results on labeled peptides confirmed that trpzip peptides are not two-state folders. This conclusion is in agreement with previous assertions that trpzip has a heterogeneous energy landscape with small energy barriers.[32−34]

**Acknowledgment.** This work was supported by a grant from the National Science Foundation (CHE03-16014, CHE07-18543 to T.A.K.), and preliminary work was developed while T.A.K. was a Fellow of the John Simon Guggenheim Memorial Foundation. The 800 MHz NMR used for part of the structural study was supported by a grant from the NSF (BIR00-79604). We are grateful for discussions with Joohyun Kim on MD results and Jan Kubelka on preliminary modeling and Ahmed Lakhani on implementing calculations, and to Heng Chi for assistance in checking spectral results.

**Supporting Information Available:** Details of the NMR structure determinations, of fits to additional thermal spectral variation studies and of spectral computations for fragments of the trpzip2 structure taken from the NMR structure and for the full peptide backbone from the TZ2C NMR structure. This material is available free of charge via the Internet at http://pubs.acs.org.

## References and Notes

(1) Cochran, A. G.; Skelton, N. J.; Starovasnik, M. A. *Proc. Natl. Acad. Sci. U.S.A.* **2001**, *98*, 5578.
(2) Ptitsyn, O. B. *FEBS Lett.* **1981**, *131*, 197.
(3) Searle, M. S.; Williams, D. H.; Rackman, L. C. *Nat. Struct. Biol.* **1995**, *2*, 999.
(4) Searle, M. S.; Zerella, R.; Williams, D. H.; Packman, L. C. *Protein Eng.* **1996**, *9*, 559.
(5) Schonbrunner, N.; Pappenberger, G.; Scharf, M.; Engles, J.; Kiefhaber, T. *Biochemistry* **1997**, *36*, 9057.
(6) Muñoz, V.; Thompson, P. A.; Hofrichter, J. *Nature* **1997**, *390*, 196.
(7) Maynard, A. J.; Sharman, G. J.; Searle, M. S. *J. Am. Chem. Soc.* **1998**, *120*, 1996.
(8) Eaton, W. A.; Muñoz, V.; Thompson, P. A.; Henry, E. R.; Hofrichter, J. *Acc. Chem. Res.* **1998**, *31*, 745.
(9) Gellman, S. H. *Curr. Opin. Chem. Biol.* **1998**, *2*, 717.
(10) Dinner, A. R.; Lazaridis, T.; Karplus, M. *Proc. Natl. Acad. Sci. U.S.A.* **1999**, *96*, 9068.
(11) Syud, F. A.; Espinosa, J. F.; Gellman, S. H. *J. Am. Chem. Soc.* **1999**, *121*, 11577.
(12) McCallister, E. L.; Alm, E.; Baker, D. *Nat. Struct. Biol.* **2000**, *7*, 669.
(13) Stanger, H. E.; Syud, F. A.; Espinosa, J. F.; Giriat, I.; Muir, T.; Gellman, S. H. *Proc. Natl. Acad. Sci. U.S.A.* **2001**, *98*, 12015.
(14) Hilario, J.; Kubelka, J.; Keiderling, T. A. *J. Am. Chem. Soc.* **2003**, *125*, 7562.
(15) Harper, J. D.; Lansbury, P. T. *Annu. Rev. Biochem.* **1997**, *66*, 385.
(16) Kelly, J. W. *Curr. Opin. Struct. Biol.* **1998**, *8*, 101.
(17) Rochet, J. C.; Lansbury, P. T. *Curr. Opin. Struct. Biol.* **2000**, *10*, 60.
(18) Nesloney, C. L.; Kelly, J. W. *Bioorg. Med. Chem.* **1996**, *4*, 739.
(19) Deechongkit, S.; Nguyen, H.; Jager, M.; Powers, E. T.; Gruebele, M.; Kelly, J. W. *Curr. Opin. Struct. Biol.* **2006**, *16*, 94.
(20) Hughes, R. M.; Waters, M. L. *Curr. Opin. Struct. Biol.* **2006**, *16*, 514.
(21) Ramírez-Alvarado, M.; Kortemme, T.; Blanco, F. J.; Serrano, L. *Bioorg. Med. Chem.* **1999**, *7*, 93.
(22) Stotz, C. E.; Topp, E. M. *J. Pharm. Sci.* **2004**, *93*, 2881.
(23) Du, D.; Tucker, M. J.; Gai, F. *Biochemistry* **2006**, *45*, 2668.
(24) Du, D.; Zhu, Y.; Huang, C.-Y.; Gai, F. *Proc. Natl. Acad. Sci. U.S.A.* **2004**, *101*, 15915.
(25) Pitera, J. W.; Haque, I.; Swope, W. C. *J. Chem. Phys.* **2006**, *124*, 141102.
(26) Smith, A. W.; Chung, H. S.; Ganim, Z.; Tokmakoff, A. *J. Phys. Chem. B* **2005**, *109*, 17025.
(27) Smith, A. W.; Tokmakoff, A. *J. Chem. Phys.* **2007**, *126*, 045109/1.
(28) Smith, A. W.; Tokmakoff, A. *Angew. Chem., Int. Ed.* **2007**, *46*, 7984.
(29) Snow, C. D.; Qiu, L.; Du, D.; Gai, F.; Hagen, S. J.; Pande, V. S. *Proc. Natl. Acad. Sci. U.S.A.* **2004**, *101*, 4077.
(30) Streicher, W. W.; Makhatadze, G. I. *J. Am. Chem. Soc.* **2006**, *128*, 30.
(31) Wang, J.; Chen, J.; Hochstrasser, R. M. *J. Phys. Chem. B* **2006**, *110*, 7545.
(32) Yang, W.-Y.; Gruebele, M. *J. Am. Chem. Soc.* **2004**, *126*, 7758.
(33) Yang, W.-Y.; Pitera, J. W.; Swope, W. C.; Gruebele, M. *J. Mol. Biol.* **2004**, *336*, 241.
(34) Hauser, K.; Krejtschi, C.; Huang, R.; Wu, L.; Keiderling, T. A. *J. Am. Chem. Soc.* **2008**, *130*, 2984.
(35) Muñoz, V.; Henry, E. R.; Hofrichter, J.; Eaton, W. A. *Proc. Natl. Acad. Sci. U.S.A.* **1998**, *95*, 5872.
(36) Wang, T.; Xu, Y.; Du, D.; Gai, F. *Biopolymers* **2004**, *75*, 163.
(37) Krejtschi, C.; Huang, R.; Keiderling, T. A.; Hauser, K. *Vib. Spectrosc.* **2008**, *48*, 1.
(38) Kubelka, J.; Huang, R.; Keiderling, T. A. *J. Phys. Chem. B* **2005**, *109*, 8231.
(39) Decatur, S. M. *Acc. Chem. Res.* **2006**, *39*, 169.
(40) Bouř, P.; Keiderling, T. A. *J. Phys. Chem. B* **2005**, *109*, 232687.
(41) Kim, J.; Huang, R.; Kubelka, J.; Bour, P.; Keiderling, T. A. *J. Phys. Chem. B* **2006**, *110*, 23590.
(42) Huang, R.; Kubelka, J.; Barber-Armstrong, W.; Silva, R. A. G. D.; Decatur, S. M.; Keiderling, T. A. *J. Am. Chem. Soc.* **2004**, *126*, 2346.
(43) Silva, R. A. G. D.; Kubelka, J.; Decatur, S. M.; Bouř, P.; Keiderling, T. A. *Proc. Natl. Acad. Sci. U.S.A.* **2000**, *97*, 8318.
(44) Santiveri, C. M.; Santoro, J.; Rico, M.; Jimenez, M. A. *J. Am. Chem. Soc.* **2002**, *124*, 14903.
(45) Kuznetsov, S. V.; Hilario, J.; Keiderling, T. A.; Ansari, A. *Biochemistry* **2003**, *42*, 4321.
(46) Lopez, M. M.; Chin, D.-H.; Baldwin, R. L.; Makhatadze, G. I. *Proc. Natl. Acad. Sci. U.S.A.* **2002**, *99*, 1298.
(47) Ahmed, Z.; Beta, I. A.; Mikhonin, A. V.; Asher, S. A. *J. Am. Chem. Soc.* **2005**, *127*, 10943.
(48) Tatko, C. D.; Waters, M. L. *J. Am. Chem. Soc.* **2002**, *124*, 9372.
(49) Zhang, J.; Qin, M.; Wang, W. *Proteins: Struct. Funct. Bioinform.* **2006**, *62*, 672.
(50) Chen, J.; Im, W.; Brooks III, C. L. *J. Am. Chem. Soc.* **2006**, *128*, 3728.
(51) Huang, R. *Infrared and circular dichroism studies of carbon-13 isotopically labeled peptide models*; University of Illinois at Chicago: Chicago, 2007.
(52) Huang, R.; Setnička, V.; Etienne, M. A.; Kim, J.; Kubelka, J.; Hammer, R. P.; Keiderling, T. A. *J. Am. Chem. Soc.* **2007**, *129*, 13592.
(53) Cochran, A. G.; Skelton, N. J.; Starovasnik, M. A. *Proc. Natl. Acad. Sci. U.S.A.* **2002**, *99*, 9081.
(54) Bouř, P.; Keiderling, T. A. *J Phys Chem. B* **2005**, *109*, 5348.
(55) Bouř, P.; Sopkova, J.; Bednarova, L.; Maloň, P.; Keiderling, T. A. *J. Comput. Chem.* **1997**, *18*, 646.

(56) Kubelka, J.; Silva, R. A. G. D.; Bour, P.; Decatur, S. M.; Keiderling, T. A. Chirality in peptide vibrations. Ab Initio computational studies of length, solvation, hydrogen bond, dipole coupling and isotope effects on vibrational CD. In *Chirality: Physical Chemistry*; Hicks, J. M., Ed.; ACS Symposium Series; American Chemical Society: Washington DC, 2002; Vol. 810, p 50.

(57) Kubelka, J.; Bouř, P.; Keiderling, T. A. Quantum Mechanical Calculations of Peptide Vibrational Force Fields and Spectral Intensities. In *Biomedical Applications of FTIR Spectroscopy*; Barth, A., Haris, P., Eds.; 2009, in press.

(58) Klamt, A.; Jonas, V.; Burger, T.; Lohrentz, J. C. W. *J. Phys. Chem. A* **1998**, *102*, 5074.

(59) Klamt, A.; Schuurmann, G. *J. Chem. Soc., Perkin Trans.* **1993**, *2*, 799.

(60) Barone, V.; Cossi, M. *J. Phys. Chem. A* **1998**, *102*, 1995.

(61) Hwang, T.; Shaka, A. J. *J. Magn. Reson.* **1995**, *112A*, 275.

(62) Xia, Youlin; Legge, G.; Jun, K.-Y.; Qi, Y.; Lee, H.; Gao, X. *Magn. Reson. Chem.* **2005**, *43*, 372.

(63) Delaglio, F.; Grzesiek, S.; Vuister, G. W.; Zhu, G.; Pfeifer, J.; Bax, A. *J. Biomol. NMR* **1995**, *6*, 277.

(64) Johnson, B. A.; Blevins, R. A. *J. Biomol. NMR* **1994**, *4*, 604.

(65) Guntert, P.; Mumenthaler, C.; Wuthrich, K. *J. Mol. Biol.* **1997**, *273*, 283.

(66) DeGuzman, R. N.; Goto, N. K.; Dyson, H. J.; Wright, P. E. *J. Mol. Biol.* **2006**, *355*, 1005.

(67) Hornak, V.; Abel, R.; Okur, A.; Strockbine, B.; Roitberg, A.; Simmerling, C. *Proteins: Struct. Funct. Bioinform.* **2006**, *65*, 712.

(68) Osapay, K.; Case, D. A. *J. Am. Chem. Soc.* **1991**, *113*, 9436.

(69) Laskowski, R. A.; Rullmann, J. A. C.; MacArthur, M. W.; Kaptein, R.; Thornton, J. M. *J. Biomol. NMR* **1999**, *8*, 477.

(70) Takekiyo, T.; Wu, L.; Yoshimura, Y.; Shimizu, A.; Keiderling, T. A. *Biochemistry*, in press.

(71) Guvench, O.; Brooks III, C. L. *J. Am. Chem. Soc.* **2005**, *127*, 4668.

(72) Wu, L.; Huang, R.; Keiderling, T. A. To be submitted for publication.

(73) Kubelka, J.; Keiderling, T. A. *J. Phys. Chem. A* **2001**, *105*, 10922.

(74) Setnicka, V.; Huang, R.; Thomas, C. L.; Etienne, M. A.; Kubelka, J.; Hammer, R. P.; Keiderling, T. A. *J. Am. Chem. Soc.* **2005**, *127*, 4992.

JP9014299